Understanding magnetic interactions in the series $A_2FeX_5 \cdot H_2O$ (A=K, Rb; X=Cl, Br). II. Inelastic neutron scattering and DFT studies

Javier Campo,[1,*] Javier Luzón,[1,2,†] Fernando Palacio,[1] Garry J. McIntyre,[2] Angel Millán,[1] and Andrew R. Wildes[2]
[1]*Instituto de Ciencia de Materiales de Aragón, CSIC-Universidad de Zaragoza, Pedro Cerbuna 12, 50009 Zaragoza, Spain*
[2]*Institut Laue-Langevin, 6 Rue Jules Horowitz, 38042 Grenoble, France*

(Received 19 February 2008; revised manuscript received 10 July 2008; published 11 August 2008)

The compounds $A_2FeX_5 \cdot H_2O$ (A=alkali or NH_4, X=Cl, Br) form a series of easy-axis antiferromagnets with transition temperatures in the range from 6 to 23 K, temperatures considerably higher than those of other similar hydrated salts of transition-metal ions. A study combining inelastic triple axis neutron spectroscopy (TAS) neutron scattering experiments and theoretical density functional theory (DFT) *ab initio* calculations of the magnetic superexchange constants has been done. A general spin-wave theory for an antiferromagnetic system with several magnetic ions in the magnetic unit cell and both uniaxial and rhombic magnetic anisotropies was employed to fit the observed magnon dispersion curves. The results obtained with the two techniques (TAS and DFT) allow us to determine with accuracy the magnetic exchange constants and therefore explain the efficiency of the superexchange pathways containing hydrogen bonds in transmitting the magnetic interactions.

DOI: 10.1103/PhysRevB.78.054415 PACS number(s): 75.50.Xx, 75.30.Et, 71.15.Mb, 78.70.Nx

I. INTRODUCTION

The study of the mechanisms governing the magnetic interactions among neighboring magnetic units represents a major goal of research in the field of molecular magnetism. A good understanding of these mechanisms would allow an improvement by crystal engineering of the efficiency in the transmission of the magnetic interactions to result in an increase of the ordering temperatures of molecular magnets. With this goal in mind we have performed a study of the magnetic interaction mechanisms in the family of easy-axis antiferromagnets $A_2FeX_5 \cdot H_2O$ (A=alkali or NH_4, X=Cl, Br). In these compounds the long superexchange pathways of the type Fe-$X\cdots X$-Fe and Fe-O$\cdots X$-Fe are surprisingly effective in transmitting the magnetic interactions, which results in relatively high transition temperatures in the range from 6 to 23 K.[1] These transition temperatures can be compared with those for other hydrated halides such as $Cs_2FeCl_5 \cdot 4H_2O$ [T_c=0.185 K (Ref. 2)], $Cs_2MnCl_4 \cdot 2H_2O$ [T_c=1.8 K (Ref. 3)], or $K_2FeF_5 \cdot H_2O$ [T_c=0.8 K (Ref. 4)] for the same type of superexchange pathways.

In a previous paper,[5] a high spin delocalization from the Fe^{3+}(S=5/2) ion toward the ligand atoms in the $A_2FeX_5 \cdot H_2O$ series has been reported. This spin delocalization reflects the delocalized nature of the magnetic molecular orbitals, which allows the magnetic interaction between different [$FeX_5 \cdot H_2O$] octahedra. Therefore, such a high spin delocalization can be considered to be responsible for the relative high transition temperatures that these compounds show.

The aim of this paper is to go a step further in our understanding of the magnetic interaction mechanisms in this series of compounds by determining the magnetic coupling constants in the same chlorine and bromine compounds ($K_2FeCl_5 \cdot H_2O$ and $Rb_2FeBr_5 \cdot H_2O$). Analysis of the five magnetic coupling constants in both compounds, particularly the comparison between magnetic interactions including and not including oxygen atoms in the superexchange pathways, will contribute to our understanding of the relative importance of two influential factors on the strength of the magnetic interaction: the spin population on the ligand atoms and the distances between the two ligand atoms in the magnetic superexchange pathways transmitting the magnetic interaction.

Therefore, in this paper, after determining all the possible magnetic interactions from an analysis of the nuclear structure we will report the study of the magnetic coupling constants by two complementary methods: inelastic triple axis neutron spectroscopy (TAS) and theoretical density functional theory (DFT) calculations. Finally in a third section we will give the conclusions of this work.

In addition, the results of this study will be related with other magnetic properties of these compounds allowing us to clarify some aspects of the rich magnetic phenomenology of this series of compounds that are briefly reviewed in the following paragraphs.

The magnetic behaviors of $K_2FeCl_5 \cdot H_2O$ and $Rb_2FeBr_5 \cdot H_2O$ have been described as the consequence of a crossover in the magnetic lattice dimensionality from one to three dimensions as temperature is decreased. The experimental results were modeled with two effective interactions: an *intrachain* interaction J_z, which corresponds to the interaction through the hydrogen bonds, and an *interchain* interaction J_{xy}, which is an average of all the other interactions and connects each chain to four neighboring ones.[6,7] The magnetic dimensionality crossover occurs when the temperature is low enough for the interchain interaction to play a competing role. The ratio between both interactions $\Re = J_{xy}/J_z$ was around 0.20–0.35 for the K compound and 0.10–0.15 for the Rb compound.

The magnetic structures of $K_2FeCl_5 \cdot H_2O$ and $Rb_2FeBr_5 . H_2O$ (Ref. 8) are described by the same magnetic unit cell as the nuclear one [(see Fig. 1(b)], with the two spins within the plane at y=0.25 aligned parallel to one another but antiparallel with respect to the spins within the plane at y=0.75. The spins are aligned parallel to the a axis. Moreover, besides the paramagnetic and the antiferromagnetic phases, these low anisotropy compounds also undergo a

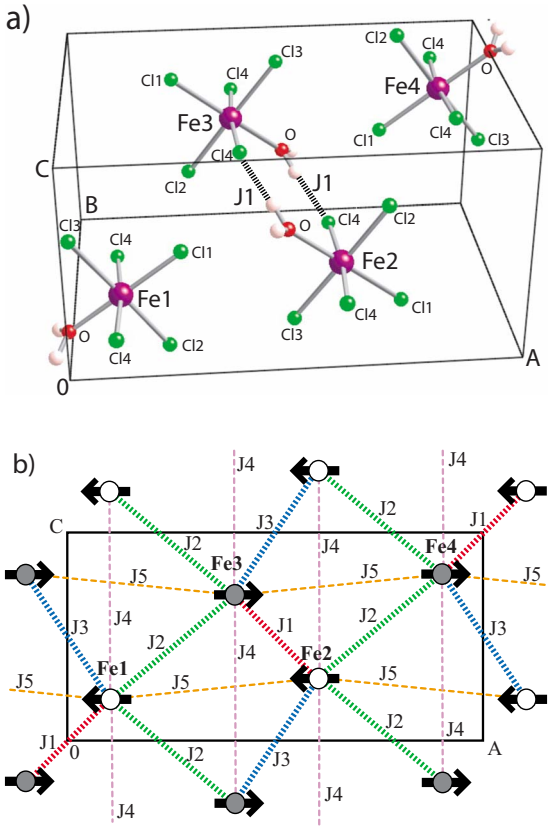

FIG. 1. (Color online) (a) Structure of $K_2FeCl_5 \cdot H_2O$. The potassium atoms have been omitted for clarity. The halogen labels are represented in all the octahedra together with the label for the four iron ions: Fe1(x,y,z), Fe2$(1/2+x,1/4,1/2-z)$, Fe3$(1/2-x,3/4,1/2+z)$, and Fe4$(-x,3/4,-z)$. (b) Scheme of the five magnetic interactions projected on the ac plane. Thick lines represent interactions connecting a Fe ion with two other Fe ions, one with $y+0.5$ and the other with $y-0.5$. The magnetic structure is also shown. White circles correspond to Fe ions with $y=1/4$ whereas gray circles $y=3/4$.

spin-flop phase[9–12] in which the spins are reoriented along the c axis at high magnetic fields.[10]

Finally, one of the most striking magnetic phenomena in this series is a remanent magnetization that appears below the antiferromagnetic transition temperature T_N.[13] The high interest of this remanent magnetization, which has also been observed in other antiferromagnetic systems,[13–16] is that it can be scaled to a universal curve independent of the compound. Although the origin of the remanent magnetization remains still unclear, the compounds showing this phenomenon seem to be Heisenberg systems with low anisotropy in which some ferromagnetic interactions, albeit often weak ones, are present.

II. DETERMINATION OF THE SUPEREXCHANGE PATHWAYS

The first step in order to study the magnetic interactions of these magnetic systems is to determine all the possible superexchange magnetic pathways that can transmit the magnetic interaction between two iron ions. This determination has been done by analyzing the nuclear structure of these compounds determined for us in a previous work,[5] in which the single-crystal neutron-diffraction techniques allowed us to locate accurately the position of the oxygen and the hydrogen atoms.

Both compounds belong to the *Pnma* space group. The unit cell contains four discrete $[FeX_5 \cdot H_2O]^{2-}$ octahedra connected by hydrogen bonds. In each octahedron three halogen atoms, the oxygen atom, and the iron atom are in special positions $4c$ with point symmetry m and the other atoms are in general positions. The octahedra are arranged in planes perpendicular to the b axis. The hydrogen bonds connect octahedra related by the inversion operator to form chains along the b axis. In this kind of structure there are five possible magnetic interactions between an iron ion and its first shell of neighbor iron ions.

Figure 1(a) represents the unit cell of $K_2FeCl_5 \cdot H_2O$, including the labeling of the halogen atoms and of the four Fe ions: Fe1(x,y,z), Fe2$(1/2+x,1/4,1/2-z)$, Fe3$(1/2-x,3/4,1/2+z)$, and Fe4$(-x,3/4,-z)$ whereas Fig. 1(b) shows a scheme of the five magnetic interactions projected on the ac plane together with the magnetic structure. These five different magnetic pathways proposed for the propagation of the magnetic interactions are also represented in Fig. 2.

The J_1 interaction propagates along the direction of the b axis through double superexchange pathways Fe-O-H$\cdots X$-Fe, linking neighboring octahedra by hydrogen bonds. This is supposed to be the strongest interaction due to the short halogen-oxygen distance and a possible enhancement of the magnetic interaction due to the hydrogen bond. In addition to J_1, there are two other interactions, J_2 and J_3, which connect iron atoms in different b planes. In both magnetic interactions the four ligand atoms involved in the magnetic pathways are halogens. The J_2 interaction is the only one with four neighbors per octahedron instead of two. This interaction propagates in planes perpendicular to the a axis, whereas the J_3 interaction propagates, similarly to J_1, in the direction of the b axis. The last two interactions connect iron atoms in the same b plane with one of the superexchange pathways of the type Fe-O$\cdots X$-Fe, but without the hydrogen bond. The J_4 interaction connects iron atoms related by the [0 0 1] translation vector and J_5 propagates parallel to the a axis.

In the superexchange pathway through the ligand atoms the strength of the magnetic interaction will depend on the distance between the closest ligand atoms. The distances between the ligand atoms involved in the superexchange pathways obtained from the nuclear structures determined by the neutron-diffraction experiments for the two compounds[5] are reported in Table I.

III. EVALUATION OF THE MAGNETIC INTERACTION CONSTANTS

The geometries of the five different magnetic interactions have been described in detail in Sec. II: in the J_1 interaction the two superexchange pathways are through a hydrogen

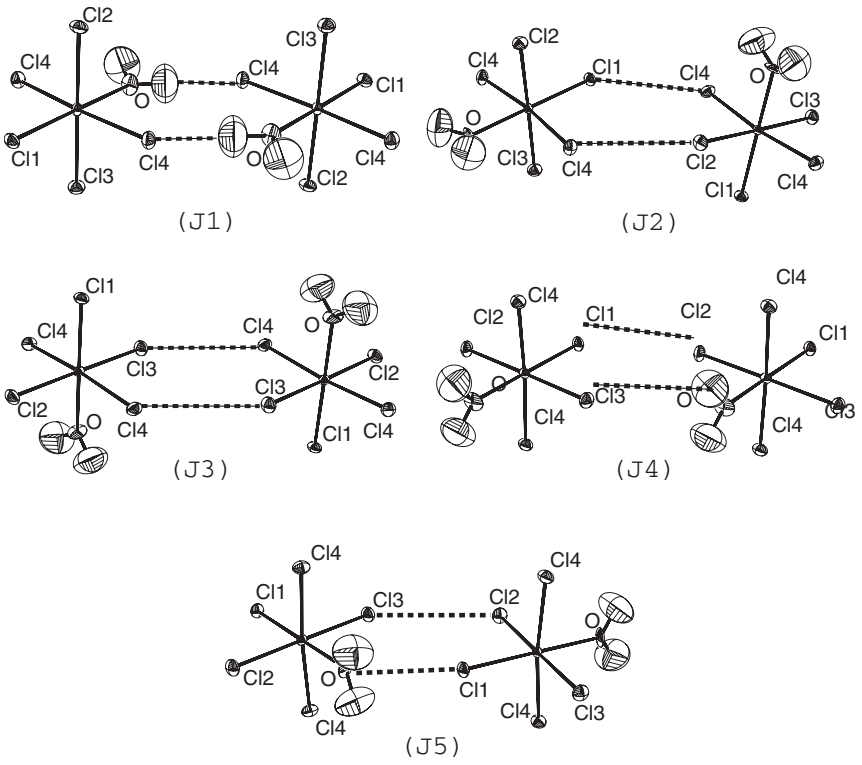

FIG. 2. Schematic view of the five proposed pathways of the magnetic interaction for $K_2FeCl_5 \cdot H_2O$.

bond between the water molecule and a halogen atom. In the J_2 and J_3 magnetic interactions there are no oxygen atoms involved in the superexchange pathways, whereas J_4 and J_5 have one superexchange pathway containing an oxygen atom, without hydrogen bonding. Before our spin-density study in the previous paper,[5] it was thought that all the relevant superexchange pathways go through the oxygen atom.[6] However, the experimental and computational spin densities show that the delocalization toward the halogen atoms is higher than toward the oxygen atom, which changes the view of the relative strengths among the magnetic interactions: J_1 must be strong since the hydrogen bond induces a halogen-oxygen contact much shorter than the other ligand-ligand contacts involved in the superexchange pathways. However, the relative strengths of the other superexchange pathways are not clear: the Fe-O$\cdots X$-Fe pathways are favored by shorter ligand-ligand distances, whereas Fe-$X\cdots X$-Fe pathways are favored by higher spin-density delocalization.

TABLE I. Distances (Å) between the ligand atoms (X=Cl, Br) involved in the superexchange pathways for $K_2FeCl_5 \cdot H_2O$ and $Rb_2FeBr_5 \cdot H_2O$ at low temperature.

Pathway	Bond	$K_2FeCl_5 \cdot H_2O$	$Rb_2FeBr_5 \cdot H_2O$
J_1	$X4$-O	3.1055(38)	3.3374(09)
	$X4$-H	2.1411(38)	2.3824(19)
J_2	$X4$-$X1$	3.7206(17)	3.9133(03)
	$X2$-$X4$	3.7934(15)	4.0362(09)
J_3	$X3$-$X4$	3.7545(15)	3.9754(51)
J_4	$X3$-O	3.8468(31)	4.0881(83)
	$X1$-$X2$	3.7100(20)	3.8750(14)
J_5	$X1$-O	3.2765(39)	3.5418(16)
	$X2$-$X3$	3.9517(19)	4.1004(21)

The knowledge of the magnetic coupling constants would allow us to appreciate the relative role played by the ligand spin populations and the ligand-ligand distances in the magnetic interactions of these compounds. A study of these magnetic coupling constants was performed by inelastic neutron scattering complemented by DFT calculations.

A. DFT calculation of the magnetic interaction constants

The computation of the five possible magnetic coupling constants for $K_2FeCl_5 \cdot H_2O$ and $Rb_2FeBr_5 \cdot H_2O$ was performed using a model in which a cluster of atoms extracted from the crystal structure is treated by an *ab initio* quantum method. This cluster included the two iron atoms involved in the magnetic interaction, their ligand atoms, and the first shell of cations around them. The correctness of this cluster model will be discussed later.

The quantum method for these calculations was the density-functional theory method in the framework of the broken-symmetry approach,[17] in which following the scheme proposed by Nagao *et al.*[18] the value for the magnetic interaction constant is

$$J = \frac{E_{BS} - E_{HS}}{\langle S^2 \rangle_{HS} - \langle S^2 \rangle_{BS}},$$

where BS denotes the broken-symmetry state and HS the high-spin state of the cluster system.

The DFT calculations were carried out with the GAUSSIAN03 software package.[19] All the calculations have employed the B3LYP density functional,[20] which has demonstrated a high degree of accuracy in the calculation of

TABLE II. BS-DFT magnetic coupling constants for the $K_2FeCl_5 \cdot H_2O$ and $Rb_2FeBr_5 \cdot H_2O$ compounds.

J	$K_2FeCl_5 \cdot H_2O$		$Rb_2FeBr_5 \cdot H_2O$	
	J (meV)	J/J_1	J (meV)	J/J_1
J_1	−0.142		−0.131	
J_2	−0.086	0.60	−0.152	1.16
J_3	−0.084	0.60	−0.154	1.17
J_4	−0.071	0.49	−0.138	0.95
J_5	−0.052	0.37	−0.063	0.48

magnetic coupling constants for other transition metals.[21] The basis set for the iron atom and the cations was the double-zeta LANL2DZ,[22] with the ECP quasirelativistic core potential for the core electrons.[23] As for the oxygen, hydrogen and halogen atoms, the polarized split-valence double-zeta Pople basis-set 6-311G** (Ref. 24) was chosen.

The magnetic coupling constants obtained through this approach are listed in Table II, where the ratio between all the interactions and the J_1 interaction is also presented.

For the analysis of these results it is useful to keep in mind the distances in the superexchange pathways listed in Table I. In the chloride compound the strongest interaction is J_1 due to the short Cl4···O distance. Among the other four interactions, the two whose superexchange pathways contain only chlorine atoms are the next-strongest ones. The superexchange pathway Fe-O···Cl3-Fe of the J_4 magnetic interaction barely contributes to the magnetic interaction due to the long O···Cl3 distance. Therefore, the relative high value of J_4, despite its having only one effective superexchange pathway, reflects the importance of the distance between the magnetic centers in the magnetic interaction, since the Cl1···Cl2 is the shortest distance between chlorine atoms involved in the magnetic pathways. In the J_5 magnetic interaction both pathways are supposed to contribute to the magnetic interaction, but they are less effective than the other Fe-Cl···Cl-Fe pathways. The Fe-Cl2···Cl3-Fe pathway has the longest Cl···Cl distance in the magnetic pathways and in the Fe-O···Cl1-Fe pathway the lower spin density of the oxygen atom is not completely compensated by the short Cl···O distance.

In the previous analysis of the magnetic interactions,[6] a simplified model was used for fitting heat capacity and magnetic-susceptibility data. In that model, there was a strong magnetic interaction in one chain (J_z) and a weaker interaction J_{xy} coupling each chain with four other chains. As mentioned above, for $K_2FeCl_5 \cdot H_2O$, a ratio J_{xy}/J_z of 0.20–0.35 was obtained. The correspondence between such a simple model and our model with five magnetic interactions is $J_z=J_1$, $J_{xy}=(J_2+2J_3-J_4-J_5)/2$, which gives a ratio of J_{xy}/J_z around 0.5, much higher than the experimental value.

In the bromide compound the distances between the two ligand atoms in the magnetic pathways are increased by around 0.2 Å in relation to the distances in the chloride compound. In the magnetic pathways, the bromine atoms compensate for this increase in the distances because the spin delocalization from the iron ion is higher and because the $3p$ bromine orbitals are more extended than the $2p$ chlorine orbitals. J_2, J_3, and J_4 are magnetic interactions whose effective pathways are of the type Fe-Br···Br-Fe, so they are increased with respect to their analogs in the chloride compound. The J_5 interaction has a Fe-O···Br-Fe pathway and a Fe-Br···Br-Fe pathway. The value of the J_5 interaction has increased but its ratio with J_2, J_3, and J_4 has decreased. Finally, the loss of efficiency in the Fe-O···Br4-Fe pathway of J_1 makes this interaction decrease and it is not the strongest one in the bromide compound.

In both compounds, the values of the magnetic interactions are in agreement with the experimental magnetic structure [see Fig. 1(b)]. The J_1, J_2, and J_3 interactions couple an iron atom with their eight nearest neighbors in different b planes. Therefore, these interactions favor b planes with ferromagnetic order in the planes but coupled antiferromagnetically between the planes. J_4 and J_5 would favor antiferromagnetic order in the b planes, but they cannot compete against the other three interactions.

B. Experimental TAS study of the magnetic coupling constants

1. TAS experiment

The inelastic neutron-scattering (INS) experiment was performed on the three-axis spectrometer IN12 at the I.L.L in Grenoble, France. A $K_2FeCl_5 \cdot D_2O$ single crystal of 1 cm^3 of volume was first mounted with the a axis vertical in order to measure the magnon dispersion curves in the b^*c^* plane and after, mounted with the b axis vertical in order to also measure a magnon dispersion curve with a component in the a^* axis. In the experiment, the final momentum of the neutron k_f was kept fixed at values of 1.2 $Å^{-1}$ near the elastic peak and 1.5 $Å^{-1}$ over the rest of the q range, whereas a Be filter was used in order to remove the $\lambda/2$ contamination. The overall energy resolutions for the two configurations were of 0.08 meV (k_f=1.2) and 0.24 meV (k_f=1.5). In order to determine the magnon dispersion curves, constant-q scans along the (0 1 ζ), (0 1+ζ 0), (0 1.5 ζ), (0 1+$\zeta\zeta$), (0 0 1+ζ), and (ζ 0 1) directions have been performed at 1.6 K, temperature much lower than the Neel temperature of 14.06 K.[25] The measurement directions in the reciprocal space were selected in order to have a correct description of the first Brillouin zone (BZ) as shown in Fig. 3(a), where the measurement directions in the first BZ together with the characteristic high-symmetry points are represented. Two of these constant-q scans are shown in Fig. 3(b) for the same point of the first BZ q=(0.00.00.1) but measured in two different directions of the reciprocal space: (0 1 ζ) and (0 0 1+ζ).

A gap in the energy is observed in the low-energy magnon branch at the center of the BZ(Γ). This gap is typical of antiferromagnetic structures with an uniaxial magnetic anisotropy. The analytical expression for this gap is[26]

$$\Delta = g\mu_B\sqrt{H_A(H_A+2H_E)},$$

where H_A is the anisotropy field, which is a hypothetical magnetic field accounting for the uniaxial magnetic anisotropy. H_E, the exchange field, represents the effect of the magnetic interactions on the magnetic ion. Both fields (H_A

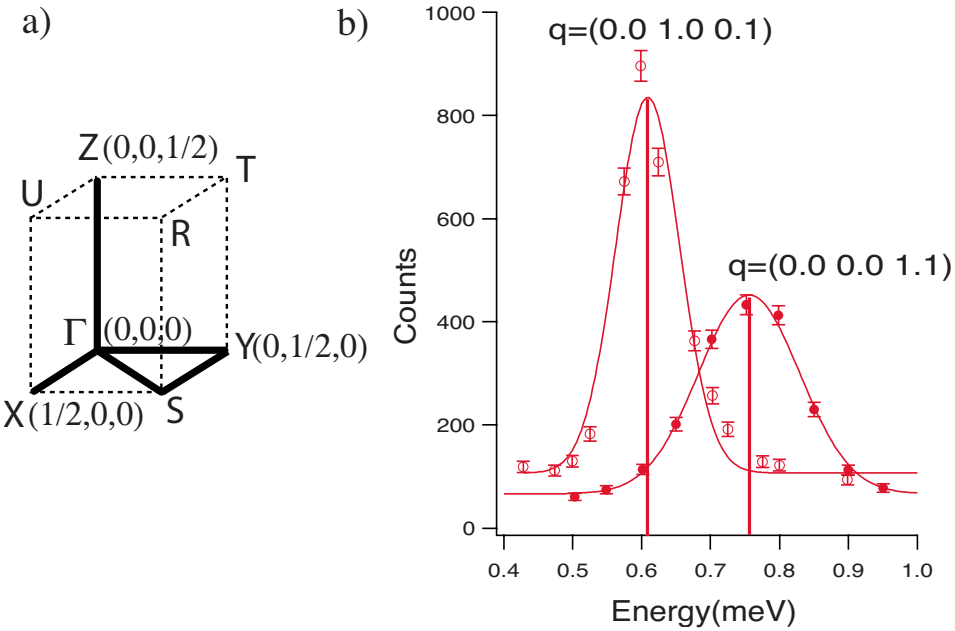

FIG. 3. (Color online) (a) High symmetry points of the first BZ together with the different directions that have been measured (thick lines). (b) Two q scans at the same point of the first BZ (0.0 0.0 0.1) but measured in different points of the reciprocal space: $q=(0.0\ 0.0\ 1.1)$ (full circles) and $q=(0.0\ 1.0\ 0.1)$ (empty circles).

$=1.7$ kOe and $H_E=199.4$ kOe) are known for $K_2FeCl_5\cdot D_2O$ from a study of the magnetic phase boundaries separating the paramagnetic, the antiferromagnetic, and the spin-flop phases[27] and allow to estimate a value for the gap of $\Delta=0.30$ meV.

This value of the gap is nearly the same as the gap observed in the magnon dispersion curves. Moreover, an additional feature in the dispersion curves is that this energy gap appears to be split in the different Brillouin zones, about 0.38 and 0.58 meV in the (0 1 0) and the (0 0 1) zones, respectively. This different gap can be graphically observed in Fig. 3(b), where two constant-q scans close to the (0 1 0) and the (0 0 1) zones are represented at the same point of the first BZ, showing an energy gap between the two inelastic peaks.

Three different models have been used in order to fit the dispersion curves and in particular the energy gaps at the center of the different Brillouin zones. The two first models consider an Heisenberg Hamiltonian with a single-ion uniaxial magnetic anisotropy; the first one neglecting the different energy gaps whereas the second one fitting the gaps with different magnon branches. Finally, in the third model a rhombic magnetic anisotropy term is introduced in order to correctly fit the different gaps.

2. Analysis and results

In a first step the dispersion curves were fitted using a linear spin-wave model where the magnetic system is described by the following Heisenberg Hamiltonian:

$$H \equiv -\sum_{i,j,\alpha,\beta} J_{i\alpha,j\beta}\mathbf{S}_{i\alpha}\cdot\mathbf{S}_{j\beta} - \sum_{i,\alpha} g_\alpha \mu_B B S^z_{i\alpha} - \sum_{i,\alpha} D_\alpha (S^z_{i\alpha})^2, \tag{1}$$

where the indices i and j designate the magnetic unit cells of the crystal and α and β denote the magnetic ions inside the magnetic unit cell. g_α is the gyromagnetic factor of the α magnetic ion, μ_B the Bohr magneton, and B the applied magnetic field parallel to the z axis. Finally, the last term accounts for an uniaxial magnetic anisotropy.

At low temperatures ($T/T_N \ll 1$), when magnetic moments present small deviation with respect to $S^z_{i\alpha}=\pm S_\alpha$($S_\alpha$ =total spin) a first-order expansion of the above anisotropic term around $S^z_{i\alpha}=\pm S_\alpha$ results in $D_\alpha(S_{i\alpha})^2 \pm 2D_\alpha S_\alpha S^z_{i\alpha}$. Therefore at low temperatures H can be rewritten as

$$H \equiv -\sum_{i,j,\alpha,\beta} J_{i\alpha,j\beta}\mathbf{S}_{i\alpha}\cdot\mathbf{S}_{j\beta} - \sum_{i,\alpha} \sigma_\alpha \mathrm{A}_\alpha S^z_{i\alpha}, \tag{2}$$

where $\sigma_\alpha=\pm 1$ represents the orientation of the spin in the z axis for the atom α of the magnetic unit cell and A_α represents the effect of a magnetic field and the uniaxial anisotropy field ($A_\alpha=\sigma_\alpha g_\alpha \mu_B B+2D_\alpha S_\alpha$).

For the Hamiltonian of Eq. (2), the possible energies of a magnon with momentum $\mathbf{k}$ are the moduli of the eigenvalues of $\sigma\mathbf{L}_\mathbf{k}$, where σ and $\mathbf{L}_\mathbf{k}$ are two matrices whose components are defined as

$$\sigma_{\alpha\beta}=\sigma_\alpha\delta_{\alpha\beta},$$

$$L_{\mathbf{k},\alpha\beta}=\left(2\sigma_\alpha\sum_{\lambda,\gamma} J_{\lambda\gamma,0\alpha}\sigma_\gamma S_\gamma + A_\alpha\right)\delta_{\alpha\beta} - 2\sigma_\alpha\sigma_\beta(S_\alpha S_\beta)^{1/2}\sum_{\lambda} J_{\lambda\beta,0\alpha}e^{i\mathbf{k}\cdot(\mathbf{X}_{\lambda,\beta}-\mathbf{X}_{0,\alpha})}, \tag{3}$$

where $\mathbf{X}_{i,\alpha}$ denotes the position of the α magnetic atom in the ith magnetic unit cell.[28,29]

The initial values of the magnetic coupling constants for the calculations were obtained from the DFT calculations plus a scale factor. At this stage (model I), only the dispersion curves in the (0 1 0) BZ were fitted. The obtained exchange magnetic coupling constants are reported in Table III. The value of the variable A_α was 0.0350 meV. The experimental and fitted dispersion curves are represented in Fig. 4. All the dispersion curves included in the refinement are well fitted, whereas the (0 0 $1+\zeta$) is well fitted away from the

TABLE III. Magnetic coupling constants for $K_2FeCl_5 \cdot D_2O$ determined from the fits to the magnon dispersion curves and the comparison with the DFT calculated magnetic coupling constants for the $K_2FeCl_5 \cdot H_2O$ and $Rb_2FeBr_5 \cdot H_2O$. Units in meV. The experimental Neel temperatures and the ones obtained from the magnetic coupling constants applying a mean-field theory are also listed.

J	Model I	Model II	Model III	DFT(K,Cl)	DFT(Rb,Br)
J_1	−0.116(4)	−0.134(6)	−0.113(3)	−0.142	−0.131
J_2	−0.040(2)	−0.062(3)	−0.037(1)	−0.086	−0.152
J_3	−0.031(3)	−0.014(4)	−0.032(3)	−0.084	−0.154
J_4	−0.021(2)	−0.021(3)	−0.023(2)	−0.071	−0.138
J_5	−0.024(3)	−0.024(4)	−0.025(2)	−0.052	−0.063
T_N	12.3 K	15.4 K	11.6 K	18.5 K	26.4 K
T_N exp. $K_2FeCl_5 \cdot H_2O$=14.1 K [a]					
T_N exp. $Rb_2FeBr_5 \cdot H_2O$=22.9 K [b]					

[a]Reference 25.
[b]Reference 1.

center of the BZ and the $(\zeta\ 0\ 1)$ is not well fitted at all, but the fitted and experimental curves do show the same behavior with respect to ζ.

A possible solution of the difference in the energy gap is that the dispersion curve observed near the center of the $(0\ 0\ 1+\zeta)$ BZ corresponds to a different magnon branch. So, in a second fit the $(0\ 0\ 1+\zeta)$ has also been considered and its dispersion curve near the BZ center has been forced to be fit by the high energy magnon branch (Model II). The exchange magnetic coupling constants obtained are also reported in Table III. The value of the variable A_α was 0.0341 meV. The experimental and fitted dispersion curves are also represented in Fig. 4. Although the problem of the difference in the energy gap has been solved, the model and the experimental dispersion curves do not fit as well as Model I in other regions and the model and experimental curves in the $(\zeta\ 0\ 1)$ zone are very different.

Each one of the spin-wave branches derived from the Hamiltonian of Eq. (2) has a twofold degeneracy. The difference in the energy gap could be due to a term not included in Eq. (2), which would break this degeneracy. Indeed, in an EPR study of the isomorphic $(NH_4)_2InCl_5 \cdot H_2O$ compound doped with Fe^{+3} ions a rhombic distortion about 20% of the uniaxial magnetic anisotropy has been observed.[30] The Hamiltonian which includes this rhombic magnetic anisotropy is

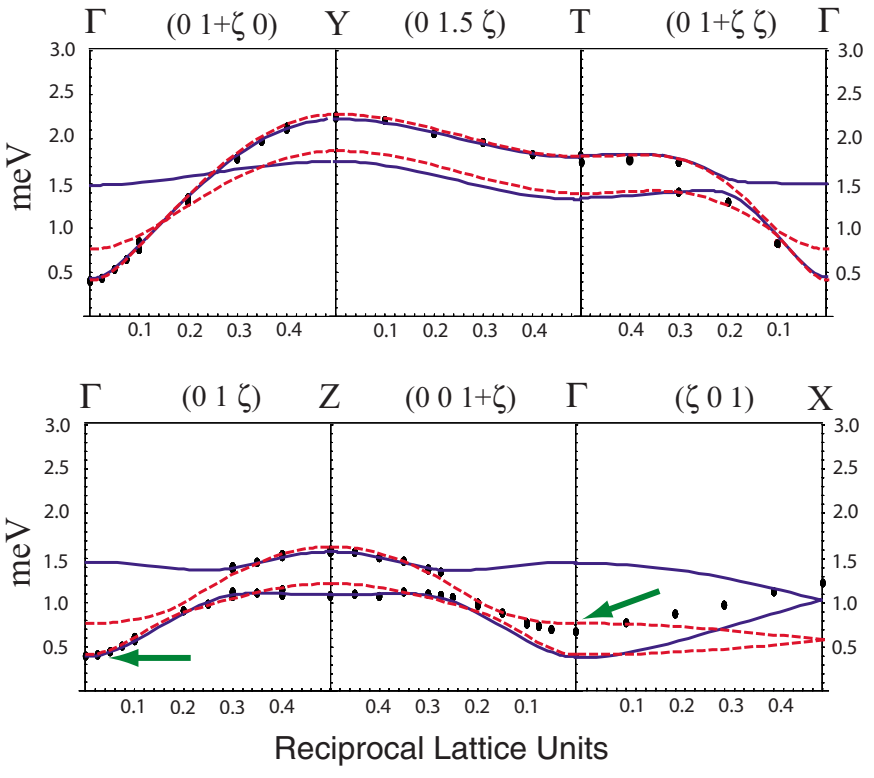

FIG. 4. (Color online) Magnon dispersion curves in $K_2FeCl_5 \cdot D_2O$. Experimental data measured at 1.6 K (dots) and best fit using model I (blue solid lines) and model II (red dashed lines). Arrows indicate the two different gaps at the Γ point.

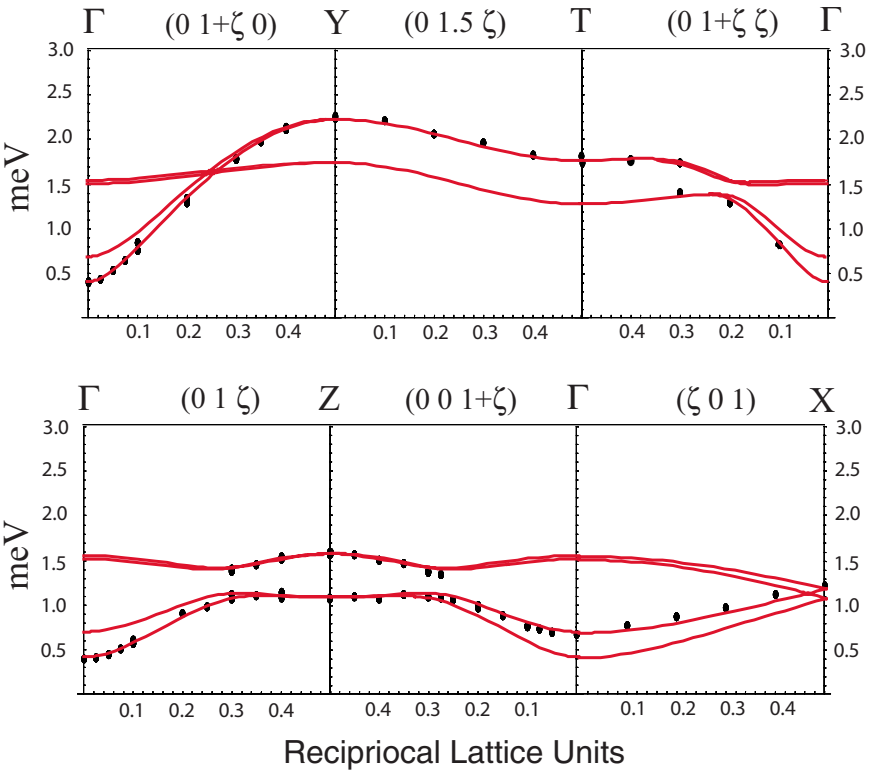

FIG. 5. (Color online). Experimental data measured at 1.6 K (dots) and best fit (solid line) of the magnon dispersion curves in $K_2FeCl_5 \cdot D_2O$ using model III in which a rhombic anisotropy term has been included.

$$H \equiv -\sum_{i,j,\alpha,\beta} J_{i\alpha,j\beta}(\mathbf{S}_{i\alpha} \cdot \mathbf{S}_{j\beta}) - \sum_{i,\alpha} \sigma_\alpha A_\alpha S_{i\alpha}^z - \sum_{i,\alpha} E_\alpha [(S_{i\alpha}^x)^2 - (S_{i\alpha}^y)^2]. \quad (4)$$

Here is important to remark that in order the previous Hamiltonian to be valid, and in particular the second term, the inclusion of the rhombic term must not change the uniaxial anisotropic nature of the magnetic ions and one of the main single-ion anisotropy axes has to be harder than the two others. This is the case of the $K_2FeCl_5 \cdot H_2O$ compound, since the existence of a spin-flop phase boundary[9–12] indicates that one of the single-ion anisotropy axes is harder than the two others.

In order to solve this Hamiltonian we have employed a linear spin-wave theory for the general case of an antiferromagnetic system with several magnetic ions in the magnetic unit cell, and with uniaxial and rhombic magnetic anisotropies. This development will be laid out later in the Appendix. For this new Hamiltonian, the possible energies of a magnon with momentum **k** are the positive values of the square root of the eigenvalues of the following matrix:

$$(\sigma \mathbf{L}_\mathbf{k} - \sigma \mathbf{N})(\sigma \mathbf{L}_\mathbf{k} + \sigma \mathbf{N}), \quad (5)$$

where σ and $\mathbf{L}_\mathbf{k}$ have been defined in Eq. (3) and the **N** matrix is defined as:

$$N_{\alpha\beta} = 2S_\alpha E_\alpha \delta_{\alpha\beta}. \quad (6)$$

All the experimental dispersion curves were included in the fit with this model (Model III). The magnetic exchange coupling constants obtained are also reported in Table III. The values of the variable A_α and E were 0.073 and 0.0072 meV, respectively, which gives a $D=0.0146$ meV. The rhombic anisotropy term (E) is around 50% of the uniaxial anisotropy term (D). This value is different from the 20% mentioned above, which was estimated from a very diluted ($x=0.03$) Fe concentration in $(NH_4)_2InCl_5 \cdot H_2O$. The experimental and fitted dispersion curves for model III are depicted in Fig. 5.

The difference in the energy gap at the Γ point of the (0 1 0) and (0 0 1) BZs can be interpreted as a breaking of the twofold degeneracy of the low-energy branch. In a model with only uniaxial anisotropy the spin fluctuations parallel to the two axes perpendicular to the easy axis are equivalent. Therefore, the introduction of the rhombic term breaks this symmetry and splits the magnon spectra (normal modes of the spin fluctuations), which are basically composed of spin fluctuations parallel to one of the two axes perpendicular to the easy axis. Therefore, the two energy gaps originated from the anisotropy between the easy axis and the two perpendicular axes. However, the intensity of the magnetic neutron scattering is proportional to the magnetic moment perpendicular to the scattering vector. In other words, near the center of the (0 1 0) BZ we observe the magnons which are basically composed of spin fluctuations parallel to the c axis, whereas near the center of the (0 0 1) BZ we observe the magnons which are basically composed of spin fluctuations parallel to the b axis. The difference in the energy gap at the center of the Brillouin zones indicates that the b axis is harder than the c axis, which is in agreement with the reorientation of the spins along the c axis in the spin-flop phase as determined by Campo *et al.*[9] This also explains why the energy gap calculated from the analysis of the magnetic phase diagram is in agreement with the energy gap of the magnon composed of spin fluctuations parallel to the c axis, since the magnetic

anisotropy considered there is the magnetic anisotropy between the *a* axis and the *c* axis, which are the directions of the spin in the antiferromagnetic phase and the spin-flop phase, respectively.

The experimental magnetic coupling constants are lower than their analogs obtained by DFT calculations. Nevertheless there is qualitative agreement in that; the experimental and DFT values are all negative and of the same order of magnitude. The main difference is the ratio between J_1 and the other magnetic interactions. The J_{xy}/J_z ratio, introduced in the section of the DFT calculations, obtained from the experimental magnetic couplings is 0.24, which is in the range 0.20–0.35 proposed in Ref. 6, whereas J_{xy}/J_z ratio from DFT calculations was around 0.5.

The differences between the DFT calculations and the experimental results can be due mainly to the very simple cluster model used in the DFT calculations, which does not account for the effect of the environment around the two octahedra. This effect on the water molecules is different to that on the chlorine atoms, which may explain the difference in the ratio J_{xy}/J_z between the experimental and the DFT coupling constants. In addition, the main magnetic pathway of the J_5 magnetic interaction is of the type Fe-O$\cdots$Cl-Fe. With respect to the other magnetic interactions, J_5 is lower in the DFT calculations than in the experimental results. Thus, it seems that the DFT calculations overestimate the importance of the Fe-Cl$\cdots$Cl-Fe magnetic pathways compared to the Fe-O$\cdots$Cl-Fe pathways.

The DFT calculations have given a correct picture of the magnetic interaction in sign, order of magnitude, and ratio among the interactions, which allows us to trust the DFT calculations on $Rb_2FeBr_5 \cdot H_2O$. However, the extrapolation of the comparison between the experimental and computational magnetic interactions for $K_2FeCl_5 \cdot H_2O$ to $Rb_2FeBr_5 \cdot H_2O$ implies that J_1 will be the strongest magnetic interaction and J_5 will be closer to the values of J_2, J_3, and J_4.

The experimental confirmation of the DFT result that all the magnetic interactions are antiferromagnetic allows us to discard the hypothesis that a necessary condition for the remnant magnetization observed in this series of compounds is the existence of ferromagnetic interactions that couple antiferromagnetic chains.[13]

Finally, an interesting test for checking the consistence of magnetic interaction values is using them for the estimation of the Neel temperatures and its comparison with the experimental ones. Considering a mean-field approach and that J_4 and J_5 are frustrated we can write the Neel temperature as $T_N = S(S+1)(2J_1+4J_2+2J_3-2J_4-2J_5)/3K_B$. The experimental Neel temperatures of both compounds together with their estimation from the different sets of magnetic interactions using the previous mean-field approach are listed in Table III showing a qualitative agreement. In the case of the DFT *J*'s, the obtained T_N are overestimated due to the overestimation of most of the magnetic interactions, as previously explained.

IV. CONCLUSIONS

A study of the magnetic interaction mechanisms in two compounds of the series $A_2FeX_5 \cdot H_2O$ (A=alkali, NH_4, X=Cl, Br) has been performed in order to understand the relatively high transition temperatures of the series.

The possible magnetic superexchange pathways have been analyzed from the precise crystallographic structure at low temperature obtained from the nonpolarized neutron-diffraction experiments reported in the accompanying paper.[5] There are five different magnetic interactions in which there are two superexchange pathways of the type either Fe-$X\cdots X$-Fe or Fe-O$\cdots X$-Fe.

The determination of the magnetic coupling constants by TAS and *ab initio* calculation has allowed us to investigate the relative effect of the spin population of the ligand atoms and the distances between the ligand atoms on the strength of the magnetic pathways. The main role of the hydrogen bond in the magnetic interaction seems to be the shortening of the O$\cdots X$ distances. In the magnetic interaction through the hydrogen bonds J_1, the short O$\cdots X$ distances compensate the low spin population of the oxygen atom and this interaction is the strongest one in both compounds. The ratio J_n/J_1 between J_1 and the other interactions is higher in the chloride compounds than in the bromide analogs and it must decrease with the size of the cation, since the size of the cation has little effect on the distance of the hydrogen bond in the J_1 magnetic pathway. However, the bigger the cation, the longer all the other distances between the ligand atoms involved in the magnetic pathways. All the magnetic interactions are negative and of the same order of magnitude.

A remarkable point is the qualitative agreement of the *ab initio* results and the experimental magnetic coupling despite the simple cluster model used for the *ab initio* calculations.

The results of this study can be related to other studies of several magnetic phenomena of this antiferromagnetic series: (i) The energy gap at the center of the BZ (Γ point) in the magnon dispersion curves is in good agreement with the energy gap calculated from an analysis of the boundaries of the magnetic phase diagram. (ii) The physical interpretation of the two different energy gaps at the Γ point in the magnon dispersion curves implies that the hardest magnetic axis is the *b* axis. This same conclusion is deduced from the magnetic structure in the spin-flop phase in which the magnetic moments are collinear to the *c* axis. (iii) The magnetic structures determined from the values of the magnetic coupling constants correspond to the experimental magnetic structure: J_1, J_2, and J_3 force an antiferromagnetic ordering between the magnetic moments located in the $y=0.25$ and $y=0.75$ *b* planes. As a consequence, the magnetic moments located in the same *b* plane are ordered ferromagnetically, although J_4 and J_5 are antiferromagnetic interactions within the *b* plane [see Fig. 1(b)]. (iv) The values of the magnetic interactions also explain the magnetic dimensionality crossover observed in the heat capacity and magnetic measurements. Indeed, in the case of $K_2FeCl_5 \cdot H_2O$ there is a quantitative agreement in the J_{xy}/J_z (defined above) with the previous analysis of the magnetic dimensionality crossover. (v) The antiferromagnetic nature of the magnetic interactions allows us to discard the hypothesis that a necessary condition for the remnant magnetization observed in this series of compounds is the existence of ferromagnetic interactions.

To sum up, this paper and paper in Ref. 5 represent an extensive study of the magnetic interaction mechanisms in

the series $A_2FeX_5 \cdot H_2O$ (A=alkali, NH_4, X=Cl, Br) by using several neutron-diffraction techniques, complemented by DFT calculations. Through the work the different magnetic coupling constants of a chloride and a bromide derivatives have been determined and the strength of the different magnetic pathways has been analyzed in function of the metal to ligand spin-density delocalization and of the ligand to ligand distances.

ACKNOWLEDGMENTS

The work in Zaragoza has been supported by the Research Grants No. MAT2006-13765-C02-02, No. MAT2007-61621, and No. CSD2007-00010 from the Ministry of Science and Innovation. The Institut Laue-Langevin is acknowledged for the allocation of neutron beam time on the instrument IN12. We are especially grateful to Mark Johnson (ILL) for advice on DFT calculations and to Jacques Previtali for technical assistance.

APPENDIX: LINEAR SPIN-WAVE THEORY

In this appendix we will develop a linear spin-wave theory for an antiferromagnetic system with several magnetic ions in the magnetic unit cell which is described by the Hamiltonian of Eq. (4), where the indices i and j designate the magnetic unit cells of the crystal and α and β denote the magnetic ions inside the magnetic unit cell. σ_α represents the orientation of the spin with respect to the z axis for the atom α of the magnetic unit cell. So, σ_α is 1 or -1. A_α can be an external magnetic field parallel to the z axis or the anisotropic field. Finally, E_α is the rhombic magnetic anisotropy of the atom α. A standard transformation for the diagonalization of the above Hamiltonian is the Holstein-Primakoff transformation,[31] where the spin operators are expressed as functions of boson operators:

$$S_{i\alpha}^x = \sqrt{S_\alpha/2}(a_{i\alpha}^+ + a_{i\alpha})f_{i\alpha},$$

$$S_{i\alpha}^y = -i\sigma_\alpha\sqrt{S_\alpha/2}(a_{i\alpha}^+ - a_{i\alpha})f_{i\alpha},$$

$$S_{i\alpha}^z = \sigma_\alpha(S_\alpha - a_{i\alpha}^+ a_{i\alpha}), \tag{A1}$$

with

$$f_{i\alpha} = [1 - a_{i\alpha}^+ a_{i\alpha}/(2S_\alpha)]^{1/2}, \tag{A2}$$

and the boson operators fulfill the usual commutation rules

$$[a_{i\alpha}, a_{j\beta}] = [a_{i\alpha}^+, a_{j\beta}^+] = 0,$$

$$[a_{i\alpha}, a_{j\beta}^+] = \delta_{ij}\delta_{\alpha\beta}.$$

In the linear spin-wave approach the approximation $f_{i\alpha}=1$ is used. The insertion of the above expressions in the Hamiltonian of Eq. (4) results in a linear spin-wave Hamiltonian:

$$\begin{aligned} H \equiv C &+ \sum_{i,j,\alpha,\beta} (2S_\beta J_{i\alpha,j\beta}\sigma_\alpha\sigma_\beta + A_\alpha\delta_{ij}\delta_{\alpha\beta})a_{i\alpha}^+ a_{i\alpha} \\ &- \sum_{i,j,\alpha,\beta} \frac{1}{2}\sqrt{S_\alpha S_\beta}J_{i\alpha,j\beta}(1+\sigma_\alpha\sigma_\beta)(a_{i\alpha}^+ a_{j\beta} + a_{i\alpha}a_{j\beta}^+) \\ &- \sum_{i,j,\alpha,\beta} \left[\frac{1}{2}\sqrt{S_\alpha S_\beta}J_{i\alpha,j\beta}(1-\sigma_\alpha\sigma_\beta) \right. \\ &\left. + S_\alpha E_\alpha \delta_{ij}\delta_{\alpha\beta}(a_{i\alpha}^+ a_{j\beta}^+ + a_{i\alpha}a_{j\beta}) \right], \end{aligned} \tag{A3}$$

where C is a constant and terms with four boson operators have been neglected since we are working in a lineal spin-wave approximation. Now, we define new variables through the Fourier transformation or inverse Fourier transformation of the boson operators:

$$q_{\mathbf{k}\alpha} = \frac{1}{N^{1/2}}\sum_i \sigma_\alpha a_{i\alpha} e^{i\sigma_\alpha \mathbf{k}\cdot\mathbf{X}_{i,\alpha}}, \tag{A4}$$

where $\mathbf{X}_{i,\alpha}$ is the position of the α magnetic atom in the i magnetic cell. These new operators obey the usual bosonic commutation relations. In the general case of $2n$ magnetic ions in the magnetic unit lattice, let us denote the magnetic ions with the spin parallel to the z axis from $\alpha=1$ to $\alpha=n$ and the magnetic ions with the spin antiparallel to the z axis from $\alpha=n+1$ to $\alpha=2n$. After some algebraic manipulations, the linear terms of Eq. (A1) can be expressed in a matrix notation as:

$$H \equiv C + \sum_{\mathbf{k}} \mathbf{Q}_\mathbf{k}^+ \mathbf{D}_\mathbf{k} \mathbf{Q}_\mathbf{k}, \tag{A5}$$

where $\mathbf{Q}_\mathbf{k}^+$ is

$$(q_{\mathbf{k}1}^+ \cdots q_{\mathbf{k}n}^+ q_{\mathbf{k}n+1} \cdots q_{\mathbf{k}2n} q_{-\mathbf{k}1} \cdots q_{-\mathbf{k}n} q_{-\mathbf{k}n+1}^+ \cdots q_{-\mathbf{k}2n}^+)$$

and $\mathbf{D}_\mathbf{k}$ is a $4n\times 4n$ matrix defined as

$$\mathbf{D}_\mathbf{k} = \begin{pmatrix} \mathbf{L}_\mathbf{k} & \mathbf{N} \\ \mathbf{N} & \mathbf{L}_\mathbf{k} \end{pmatrix}, \tag{A6}$$

with $\mathbf{L}_\mathbf{k}$ and $\mathbf{N}$ both $2n\times 2n$ matrices defined in Eqs. (3) and (6)

We can define new operators as

$$\phi_{\mathbf{k}\alpha} = q_{\mathbf{k}\alpha} \quad \alpha = 1, \cdots, n,$$

$$\phi_{\mathbf{k}\alpha} = q_{\mathbf{k}\alpha}^+ \quad \alpha = n+1, \cdots, 2n,$$

$$\phi_{\mathbf{k}\alpha} = q_{-\mathbf{k}\alpha-n}^+ \quad \alpha = 2n+1, \cdots, 3n,$$

$$\phi_{\mathbf{k}\alpha} = q_{-\mathbf{k}\alpha-n} \quad \alpha = 3n+1, \cdots, 4n, \tag{A7}$$

for which we have the commutation rules:

$$[\phi_{\mathbf{k}\alpha}, \phi_{\mathbf{k}\beta}] = [\phi_{\mathbf{k}\alpha}^+, \phi_{\mathbf{k}\beta}^+] = 0,$$

$$[\phi_{\mathbf{k}\alpha}, \phi_{\mathbf{k}\beta}^+] = \Lambda_{\alpha\beta}, \tag{A8}$$

with $\sigma_{\alpha\beta}=\sigma_\alpha\delta_{\alpha\beta}$ $\alpha,\beta=1,\cdots,2n$ and

$$\Lambda = \begin{pmatrix} \sigma & \\ & -\sigma \end{pmatrix}.$$

With these new operators the Hamiltonian can be written as

$$H \equiv C + \sum_{\mathbf{k}} \Phi_{\mathbf{k}}^{+} \mathbf{D}_{\mathbf{k}} \Phi_{\mathbf{k}}, \tag{A9}$$

where

$$\Phi_{\mathbf{k}}^{+} \equiv (\phi_{\mathbf{k}1}^{+}, \ldots, \phi_{\mathbf{k}4n}^{+}). \tag{A10}$$

Let us consider now the equation of motion for the vectorial operator $\Phi_{\mathbf{k}}$. From Eq. (A9) and the commutation rules of Eq. (A8) we have:

$$\frac{d\Phi_{\mathbf{k}}}{dt} = i[H, \Phi_{\mathbf{k}}] = -i\Lambda \mathbf{D}_{\mathbf{k}} \Phi_{\mathbf{k}}, \tag{A11}$$

whose explicit solution is

$$\Phi_{\mathbf{k}}(t) = e^{-i\Lambda \mathbf{D}_{\mathbf{k}} t} \Phi_{\mathbf{k}}(0). \tag{A12}$$

Therefore, the energy of the magnons will be the modulus of the eigenvalues of the matrix $\Lambda \mathbf{D}_{\mathbf{k}}$,

$$\Lambda \mathbf{D}_{\mathbf{k}} = \begin{pmatrix} \sigma \mathbf{L}_{\mathbf{k}} & \sigma \mathbf{N} \\ -\sigma \mathbf{N} & -\sigma \mathbf{L}_{\mathbf{k}} \end{pmatrix}. \tag{A13}$$

Finally, these energies can be obtained as the positive square root of the eigenvalues of the following matrix:

$$(\sigma \mathbf{L}_{\mathbf{k}} - \sigma \mathbf{N})(\sigma \mathbf{L}_{\mathbf{k}} + \sigma \mathbf{N}), \tag{A14}$$

which is the result that has been used in the experimental section.

*Corresponding author: jcampo@unizar.es
†Present address: Laboratory of Molecular Magnetism, Via della Lastruccia 3, Sesto Fiorentino(FI), 50019 Italy.

[1] R. L. Carlin, S. N. Bhatia, and C. J. O'Connor, J. Am. Chem. Soc. **99**, 7728 (1977).
[2] R. L. Carlin and R. Burriel, Phys. Rev. B **27**, 3012 (1983).
[3] T. Smith and S. A. Friedberg, Phys. Rev. **177**, 1012 (1969).
[4] R. L. Carlin, R. Burriel, J. A. Rojo, and F. Palacio, Inorg. Chem. **23**, 2213 (1984).
[5] J. Luzon, J. Campo, F. Palacio, G. J. McIntyre, and A. Millan, the preceding paper, Phys. Rev. B **78**, 054414 (2008).
[6] J. A. Puertolas, R. Navarro, F. Palacio, J. Bartolome, D. Gonzalez, and R. L. Carlin, Phys. Rev. B **31**, 516 (1985).
[7] J. A. Puertolas, R. Navarro, F. Palacio, J. Bartolome, D. Gonzalez, and R. L. Carlin, Phys. Rev. B **26**, 395 (1982).
[8] M. Gabás, F. Palacio, J. Rodríguez-Carvajal, and D. Visser, J. Phys.: Condens. Matter **7**, 4725 (1995).
[9] J. Campo, F. Palacio, M. C. Morón, C. Becerra, and A. Paduan-Filho, J. Phys.: Condens. Matter **11**, 4409 (1999).
[10] J. Campo, F. Palacio, A. Paduan-Filho, C. Becerra, M. Fernández-Díaz, and J. Rodríguez-Carvajal, Physica B (Amsterdam) **234-236**, 622 (1997).
[11] A. Paduan-Filho, F. Palacio, and R. L. Carlin, J. Phys. (Paris), Lett. **39**, L279 (1978).
[12] F. Palacio, A. Paduan-Filho, and R. L. Carlin, Phys. Rev. B **21**, 296 (1980).
[13] C. C. Becerra, A. Paduan-Filho, T. Fries, Y. Shapira, M. Gabás, J. Campo, and F. Palacio, J. Magn. Magn. Mater. **140-144**, 1475 (1995).
[14] T. Fries, Y. Shapira, A. Paduan-Filho, C. Becerra, and F. Palacio, J. Phys.: Condens. Matter **5**, L107 (1993).
[15] Z. V. Carvalho, C. C. Becerra, A. Paduan-Filho, and F. Palacio, J. Magn. Magn. Mater. **226-230**, 615 (2001).
[16] F. Palacio, M. Gabás, J. Campo, C. C. Becerra, A. Paduan-Filho, and V. B. Barbeta, Phys. Rev. B **56**, 3196 (1997).
[17] L. Noodleman and J. G. Norman, J. Chem. Phys. **70**, 4903 (1979).
[18] H. Nagao, M. Nishino, Y. Shigeta, T. Soda, Y. Kitagawa, T. Onishi, Y. Yoshioka, and K. Yamaguchi, Coord. Chem. Rev. **198**, 265 (2000).
[19] M. J. Frisch *et al.*, GAUSSIAN 03, Revision C.02, Gaussian, Inc., Wallingford, CT, 2004.
[20] A. D. Becke, J. Chem. Phys. **98**, 5648 (1993).
[21] I. Ciofini and C. A. Daul, Coord. Chem. Rev. **238-239**, 187 (2003).
[22] N. C. Handy and H. F. Schaefer, J. Chem. Phys. **81**, 5031 (1984).
[23] W. R. Wadt and P. J. Hay, J. Chem. Phys. **82**, 284 (1985).
[24] R. Krishnan, J. S. Binkley, R. Seeger, and J. A. Pople, J. Chem. Phys. **72**, 650 (1980).
[25] J. N. McElearney and S. Merchant, Inorg. Chem. **17**, 1207 (1978).
[26] R. L. Carlin and A. J. van Duyneveldt, *Magnetic Properties of Transition Metal Compounds* (Springer-Verlag, New York, 1977).
[27] R. L. Carlin and F. Palacio, Coord. Chem. Rev. **65**, 141 (1985).
[28] A. W. Saenz, Phys. Rev. **125**, 1940 (1962).
[29] T. Masuda, A. Zheludev, B. Grenier, S. Imai, K. Uchinokura, E. Ressouche, and S. Park, Phys. Rev. Lett. **93**, 077202 (2004).
[30] S. K. Misra and G. R. Sharp, J. Chem. Phys. **66**, 4172 (1977).
[31] T. Holstein and H. Primakoff, Phys. Rev. **58**, 1098 (1940).